*Inorg. Chem.* **2005**, *44*, 187−196


# Synthesis, Crystal Structure, and High-Precision High-Frequency and -Field Electron Paramagnetic Resonance Investigation of a Manganese(III) Complex: $[Mn(dbm)_2(py)_2](ClO_4)$

**Guillem Aromí,[†] Joshua Telser,[‡] Andrew Ozarowski,[§] Louis-Claude Brunel,[§] Helen-Margaret Stoeckli-Evans,[||] and J. Krzystek*[,§]**

*Departament de Química Inorgànica, Facultat de Química, Universitat de Barcelona, E-08028 Barcelona, Spain, Chemistry Program, Roosevelt University, Chicago, Illinois 60605, National High Magnetic Field Laboratory, Florida State University, Tallahassee, Florida 32310, and Laboratoire de Cristallographie, Institut de Chimie, Université de Neuchâtel, CH-2007 Neuchâtel, Switzerland*

Received June 23, 2004

The complex $[Mn(dbm)_2(py)_2](ClO_4)$ (dbm = anion of 1,3-diphenyl-1,3-propanedione (dibenzoylmethane), py = pyridine) was synthesized and characterized by X-ray crystallography. It has tetragonally distorted geometry with the axial positions occupied by the py ligands and the equatorial positions by the dbm ligands. This mononuclear complex of high-spin Mn(III) ($3d^4$, $S = 2$) was studied by high-frequency and -field electron paramagnetic resonance (HFEPR) both as a solid powder and in frozen dichloromethane solution. Very high quality HFEPR spectra were recorded over a wide range of frequencies. The complete dataset of resonant magnetic fields versus transition energies was analyzed using automated fitting software. This analysis yielded the following spin Hamiltonian parameters (energies in $cm^{-1}$): $D = -4.504(2)$, $E = -0.425(1)$, $B_4^0 = -1.8(4) \times 10^{-4}$, $B_4^2 = 7(3) \times 10^{-4}$, $B_4^4 = 48(4) \times 10^{-4}$, $g_x = 1.993(1)$, $g_y = 1.994(1)$, and $g_z = 1.983(1)$, where the $B_4^n$ values represent fourth-order zero-field splitting terms that are generally very difficult to extract, even from single-crystal measurements. The results here demonstrate the applicability of HFEPR at high-precision measurements, even for powder samples. The zero-field splitting parameters determined here for $[Mn(dbm)_2(py)_2]^+$ are placed into the context of those determined for other mononuclear complexes of Mn(III).

## Introduction

Ever since the first successful application of high-frequency and -field electron paramagnetic resonance (HFEPR)[1] in 1997 to detect paramagnetic resonances in high-spin Mn(III) ($3d^4$, $S = 2$),[2,3] this formerly "EPR-silent" ion has been studied in a variety of molecular complexes representing different coordination numbers and geometries. The original HFEPR detection involved, in one case, five-coordinated porphyrinic complexes, Mn(TPP)Cl and its porphyrazine analogues,[2] representing a square-pyramidal coordination sphere of the type $N_4Cl$, and, in the other, a six-coordinate complex, $Mn(dbm)_3$ (where Hdbm is dibenzoylmethane, formally, 1,3-diphenyl-1,3-propanedione), representing a distorted octahedral geometry of exclusively oxygen donors ($O_6$).[3] Mn(III) with $O_6$ coordination had also been studied early on by EPR[4] and quite recently by INS,[5] as well as by HFEPR.[6] Related, five-coordinate complexes with $O_4Cl$ and $O_4Br$ donors have been studied by HFEPR

* Author to whom correspondence should be addressed. E-mail: krzystek@magnet.fsu.edu. Phone: +1 850 644 6077. Fax: +1 850 644 9462.
[†] Universitat de Barcelona.
[‡] Roosevelt University.
[§] Florida State University.
[||] Université de Neuchâtel.

(1) Abbreviations used: acac, anion of 2,4-pentanedione (acetylacetone); dbm, anion of 1,3-diphenyl-1,3-propanedione (dibenzoylmethane); EPR, electron paramagnetic resonance; HFEPR, high-frequency and -field EPR; INS, inelastic neutron scattering; NIR, near infrared; OEP, dianion of octaethylporphine; py, pyridine; rms, root-mean-square error; TPP, dianion of *meso*-tetraphenylporphine; zfs, zero-field splitting.

(2) Goldberg, D. P.; Telser, J.; Krzystek, J.; Montalban, A. G.; Brunel, L.-C.; Barrett, A. G. M.; Hoffman, B. M. *J. Am. Chem. Soc.* **1997**, *119*, 8722−8723.
(3) Barra, A.-L.; Gatteschi, D.; Sessoli, R.; Abbati, G. L.; Cornia, A.; Fabretti, A. C.; Uytterhoeven, M. G. *Angew. Chem., Intl. Ed. Engl.* **1997**, *36*, 2329−2331.
(4) Gerritsen, H. J.; Sabisky, E. S. *Phys. Rev.* **1963**, *132*, 1507−1512.

10.1021/ic049180u CCC: $30.25 
Published on Web 12/16/2004

as well.[7] Further work has been reported on the properties of complexes with nitrogen donor ligands. These include porphyrinic complexes of Mn(III) with varying axial ligation: $N_4$;[8] $N_4O$;[9] $N_4X$ (X = Cl,[10] Br[7]). Six-coordinate complexes with all nitrogen donors ($N_6$)[11] and various mixed nitrogen and halide donors ($N_3F_3$)[12] and $N_4X_2$ (X = Br, I)[13,14] have also been studied. Last, a five-coordinate complex with the mixed donor set $N_2O_2Cl$ has also been investigated by low-frequency EPR[15] and HFEPR.[16] Given the number of complexes studied, qualitative and quantitative conclusions can already be drawn about their magnetic properties as well as electronic vs geometric structure (see Discussion). The principal aim of this study is thus to characterize structurally and spectroscopically, chiefly by HFEPR, a mononuclear Mn(III) complex with an $N_2O_4$ coordination sphere, which is a type hitherto not studied, to our best knowledge. This was realized by synthesizing and investigating the complex $[Mn(dbm)_2(py)_2](ClO_4)$, subsequently termed **1**.

The coordination environment of Mn(III) in **1** is of particular interest with respect not only to other six-coordinate complexes of Mn(III) described above but also because so many of the Mn(III) complexes thus far characterized contain equatorial $N_4$ donor ligands (i.e., tetrapyrroles[8−10,17] and saturated tetraazamacrocycles[13,14]) with various weaker field, axial ligands. In this study, **1** has an equatorial $O_4$ donor set and axial nitrogen donors. The two dbm ligands do not comprise a macrocycle, but each is $\pi$-conjugated and, taken together, the result is equatorial ligation that could be described as an $O_4$ "porphyrinoid".

Concerning the spectroscopic characterization, of particular attention was the possibility to increase the accuracy in determining the spin Hamiltonian parameters describing the $S = 2$ spin state of Mn(III), in particular the fourth-order zfs terms. This advance proved possible thanks to the very high quality of the HFEPR spectra obtained from polycrystalline solid samples. To the best of our knowledge, this is the first time that fourth-order zfs terms have been accurately determined for a mononuclear high-spin Mn(III) complex from *powder* spectra.

## Experimental Section

**Synthesis.** All manipulations were performed in air using reagents as received. $Bu^n_4NMnO_4$ was prepared[18] as reported in the literature.[19] To a stirred light yellow solution of $Mn(ClO_4)_2 \cdot 6H_2O$ (450 mg, 1.24 mmol) and pyridine (3 mL, 37.09 mmol) in MeCN (15 mL) was added dropwise a purple solution of freshly prepared $Bu^n_4NMnO_4$ (111 mg, 0.31 mmol) in MeCN (2 mL). Solid Hdbm (700 mg, 3.13 mmol) was added immediately to the resulting dark brown solution, and the mixture was stirred for a few hours, after which a brown precipitate of $[Mn(dbm)_2(py)_2](ClO_4)$ (**1**) had formed. The solid was collected by filtration, washed with $Et_2O$, and dried under vacuum. The yield was ∼50%.

IR (neat): $\nu$ ($cm^{-1}$) = 1599.3 m, 1585.6 w, 1511.4 vs, 1484.8 vs, 1445.9 m, 1433.9 m 1341.1 s, 1321.7 s, 1230.4 m, 1185.9 w, 1159.6 m, 1094.2 vs, 1067.3 m, 1022.7 m, 1007.9 w, 1000.0 w, 940.2 w, 762.9 w, 748.2 w, 726.4 w, 705.5 m, 685.9 w, 622.2 m, 589.6 w, 552.0 w, 422.1 w.

Anal. Calcd for **1** ($M_r$ = 759.10): C, 63.29; H, 4.25; N, 3.69; Mn, 7.24. Found: C, 63.31; H, 4.10; N, 3.67; Mn, 7.27. Large crystals suitable for X-ray crystallography could be obtained overnight if the stirring was interrupted just a few minutes after the addition of Hdbm and the system was left unperturbed.

**X-ray Crystallography.** Suitable crystals of **1** were obtained as dark brown rods. The intensity data were collected at 153 K (−120 °C) on a Stoe Mark II image plate diffraction system equipped with a two-circle goniometer and using Mo Kα graphite-monochromated radiation. The image plate distance was 100 mm, and $\omega$ rotation scans were conducted with angles of 0−180° at $\phi$ 0° and 0−64° at $\phi$ 90°, with a step $\Delta\omega = 1.0°$. The $2\theta$ range was 2.29−59.53°, and $d_{max}-d_{min}$ was 17.779−0.716 Å. The structure was solved by direct methods using the program SHELXS-97.[20] The refinement and all further calculations were carried out using SHELXL-97.[21] The H atoms were located from Fourier difference maps and refined isotropically. The non-H atoms were refined anisotropically, using weighted full-matrix least squares on $F^2$. The molecular structure and crystallographic numbering scheme are illustrated in Figure 1.

**HFEPR.** The experiments were performed using a single-pass transmission-type spectrometer, in which the sub-THz waves are propagated in cylindrical lightpipes, as described previously.[22] Sub-THz frequencies were generated by either of two Gunn oscillators, operating at 95 ± 3 and 110 ± 3 GHz, respectively. In addition to the fundamentals, the frequencies were also multiplied by factors of 2−4 using Schottky diode-based multipliers. The power emitted varied strongly with the harmonic generated this way. A 17 T superconducting magnet from Oxford Instruments was used. The magnetic field values were read from the power supply current through proper calibration. Errors associated with this procedure


(5) Basler, R.; Tregenna-Piggott, P. L. W.; Andres, H.; Dobe, C.; Güdel, H.-U.; Janssen, S.; McIntyre, G. J. *J. Am. Chem. Soc.* **2001**, *123*, 3377−3378.
(6) Krzystek, J.; Yeagle, G.; Park, J.-H.; Meisel, M. W.; Britt, R. D.; Brunel, L.-C.; Telser, J. *Inorg. Chem.* **2003**, *42*, 4610−4618.
(7) Krzystek, J.; Telser, J.; Knapp, M. J.; Hendrickson, D. N.; Aromi, G.; Christou, G.; Angerhofer, A.; Brunel, L.-C. *Appl. Magn. Reson.* **2001**, *23*, 571−585.
(8) Krzystek, J.; Telser, J.; Hoffman, B. M.; Brunel, L.-C.; Licoccia, S. *J. Am. Chem. Soc.* **2001**, *123*, 7890−7897.
(9) Bendix, J.; Gray, H. B.; Golubkhov, G.; Gross, Z. *J. Chem. Soc., Chem. Commun.* **2000**, 1957−1958.
(10) Krzystek, J.; Telser, J.; Pardi, L. A.; Goldberg, D. P.; Hoffman, B. M.; Brunel, L.-C. *Inorg. Chem.* **1999**, *38*, 6121−6129.
(11) Limburg, J.; Vrettos, J. S.; Crabtree, R. H.; Brudvig, G. W.; de Paula, J. C.; Hassan, A.; Barra, A.-L.; Duboc-Toia, C.; Collomb, M.-N. *Inorg. Chem.* **2001**, *40*, 1698−1703.
(12) Mantel, C.; Hassan, A. K.; Pécaut, J.; Deronzier, A.; Collomb, M.-N.; Duboc-Toia, C. *J. Am. Chem. Soc.* **2003**, *125*, 12337−12344.
(13) Mossin, S.; Weihe, H.; Barra, A.-L. *J. Am. Chem. Soc.* **2002**, *124*, 8764−8765.
(14) Mossin, S.; Stefan, M.; ter Heerdt, P.; Bouwen, A.; Goovaerts, E.; Weihe, H. *Appl. Magn. Reson.* **2002**, *21*, 586.
(15) Campbell, K. A.; Lashley, M. R.; Wyatt, J. K.; Nantz, M. H.; Britt, R. D. *J. Am. Chem. Soc.* **2001**, *123*, 5710−5719.
(16) Krzystek, J.; Telser, J. *J. Magn. Reson.* **2003**, *162*, 454−465.
(17) Krzystek, J.; Pardi, L. A.; Brunel, L.-C.; Goldberg, D. P.; Hoffman, B. M.; Licoccia, S.; Telser, J. *Spectrochim. Acta, Part A* **2002**, *58*, 1113−1127.
(18) **Warning!** *There have been reports of a detonation of quaternary ammonium permanganates during drying at elevated temperature. We recommend appropriate care be taken in the use of organic permanganates. The* $Bu^n_4N^+$ *salt should be dried in vacuo at room temperature.*
(19) Vincent, J. B.; Folting, K.; Huffman, J. C.; Christou, G. *Inorg. Chem.* **1996**, *25*, 996−999.
(20) Sheldrick, G. M. *Acta Crystallogr.* **1990**, *A46*, 467−473.
(21) Sheldrick, G. *SHELXL*; University of Göttingen: Göttingen, Germany, 1999.
(22) Hassan, A. K.; Pardi, L. A.; Krzystek, J.; Sienkiewicz, A.; Goy, P.; Rohrer, M.; Brunel, L.-C. *J. Magn. Reson.* **2000**, *142*, 300−312.

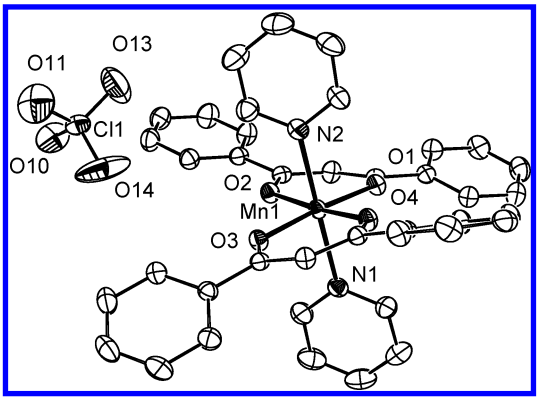


**Figure 1.** ORTEP plot of **1** at 50% probability level. Hydrogen atoms have been omitted for clarity.

are discussed elsewhere.[22] Temperature control was achieved with an Oxford Instruments CF1200 continuous-flow liquid-helium cryostat and an IC503 controller. Field modulation and the ensuing phase-sensitive detection using a Stanford SR830 lock-in amplifier was applied. Experiments were performed on either polycrystalline solid or a solution in $CH_2Cl_2$ (Aldrich-Sigma, analytical grade). In the second case, the solvent was purged with nitrogen to reduce the concentration of dissolved oxygen, which often produces strong HFEPR signals at low temperatures.[23] An attempt to apply toluene as a glassing agent to improve the frozen solvent quality[16] resulted in precipitating the complex and was therefore abandoned. The $CH_2Cl_2$ solution was of sufficiently high quality, judging by the obtained spectra. Typically, 20−30 mg of the sample was used in either the solid-state or solution measurement. In addition, a conventional X-band EPR experiment was performed on both solid and solution sample.

**Other Physical Measurements.** FTIR spectra were collected on a Perkin-Elmer Spectrum RXI spectrometer. $^1$H NMR spectra were recorded on a 250 MHz Bruker DRX 250 spectrometer. Elemental analyses were performed with a Carlo Erba Instruments CHNS-O EA-1108 elemental analyzer. UV/vis/NIR spectra were recorded on a Jasco V-570 spectrophotometer. Compound **1** in $CH_2Cl_2$ solution exhibits a very strong charge-transfer band below 450 nm, a band at 480 nm ($\epsilon = 1550$ M$^{-1}$ cm$^{-1}$), and shoulders at 505 and 520 nm. No absorption was observed above 700 nm.

**Theory for EPR Spectra.** To analyze the EPR spectra, we applied the most general spin Hamiltonian for an $S = 2$ spin state including both the second-order and the fourth-order terms of the zero-field splitting:[24]

$$\mathscr{H} = \beta B\cdot\mathbf{g}\cdot S + B_2^0O_2^0 + B_2^2O_2^2 + B_4^0O_4^0 + B_4^2O_4^2 + B_4^4O_4^4 \quad (1a)$$

In the following discussion we will apply the commonly used second-order zfs parameters $D \equiv 3B_2^0$ and $E \equiv B_2^2$ while retaining the form of the fourth-order terms as shown above:

$$\mathscr{H} = \beta B\cdot\mathbf{g}\cdot S + D(S_z^2 - S(S+1)/3) + E(S_x^2 - S_y^2) + B_4^0O_4^0 + B_4^2O_4^2 + B_4^4O_4^4 \quad (1b)$$

The operators $O_4^m$ as well as their matrix elements may be found in many texts including Abragam and Bleaney.[24,25] The zero-field energy levels resulting from this spin Hamiltonian acting on quintet state wave functions are shown in Figure 2. A spin Hamiltonian for $S = 2$ can also include higher order field-dependent (Zeeman) terms, such as $B\cdot S^3$,[26] which can complicate determination of $g$ values; however, it was not necessary to consider such terms here.

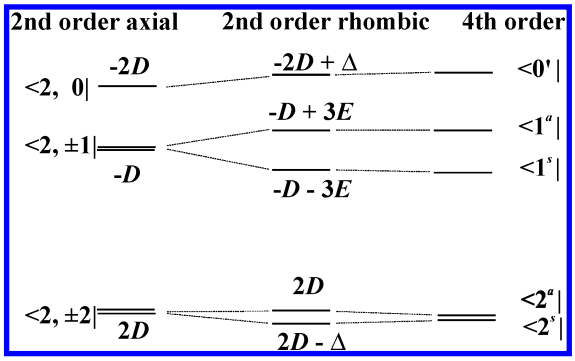


**Figure 2.** Effect of particular zero-field splitting terms of the spin Hamiltonian (eq 1) acting on quintet state wave functions. $\Delta = 3E^2/D$.

**Least-Squares Fitting Procedure.** Single-frequency powder spectra were simulated using a locally written program (available from A.O.). The transition probabilities were calculated from the eigenvectors in a standard way.[27] The calculated transition intensities were corrected for the Boltzmann populations of the levels involved because of the relatively large values of the zfs parameters and the high magnetic fields at which certain transitions occurred. After finding by the trial-and-error method the initial parameters $\boldsymbol{g}$, $D$, and $E$ that gave reasonable powder simulations, all transitions observed in the experimental powder spectra were identified as corresponding to the $x$, $y$, $z$ or to the off-axial turning points. A 2-dimensional array whose rows contained frequency (in the range of ∼90−440 GHz), polar angles Θ and Φ, and resonance field was used as our input data. This array was simultaneously fitted by use of a nonlinear least-squares (Simplex) method to minimize the function

$$\chi^2 = \sum_{i=1}^{N}(f_i^{(\mathrm{calc})} - f_i^{(\mathrm{exp})})^2 \quad (2)$$

where $f_i$ are the calculated and experimental resonance fields. Because we assumed (and confirmed in separate experiments described in ref 22) that all experimental resonance fields bear approximately the same uncertainty, there was no need to include uncertainties $\sigma^2_i$ in the denominator. The resonance fields $f_i^{(\mathrm{calc})}$ were evaluated using the same Householder method[28] to diagonalize the spin Hamiltonian in eq 1 that the powder simulation had employed, but no transition probabilities nor Boltzmann factors were calculated in this case. The least-squares procedure was carried out in conjunction with human judgment, which was used to eliminate mathematically possible, but unphysical, results to obtain best-fit parameters for the entire field vs energy 2-D array of EPR transitions. After convergence had been achieved, the Hessian

(23) Pardi, L. A.; Krzystek, J.; Telser, J.; Brunel, L.-C. *J. Magn. Reson.* **2000**, *146*, 375−378.
(24) Abragam, A.; Bleaney, B. *Electron Paramagnetic Resonance of Transition Ions*; Dover Publications: New York, 1986.
(25) Sometimes, a different set of fourth-order zfs terms is used, comprising parameters $a$ and $F$. Parameter $a$ is equal to $120B_4^0$ or $24B_4^4$ in a cubic environment. Parameter $F$ reflects deviation from the perfect cubic symmetry and is equal to $36B_4^4 - 180B_4^0$.
(26) McGavin, D. G.; Tennant, W. C.; Weil, J. A. *J. Magn. Reson.* **1990**, *87*, 92−109.
(27) Bencini, A.; Gatteschi, D. In *Transition Metal Chemistry*; Melson, G. A., Figgis, B. N., Eds.; Marcel Dekker: New York, 1982; Vol. 8, p 1.
(28) Press: W. H.; Flannery, B. P.; Teukolsky, A. A.; Vetterling, W. T. In *Numerical Recipes in Pascal*; Cambridge University Press: Cambridge, U.K., 1989; p 572.

matrix was calculated. The Hessian matrix[29] is formally a matrix containing the second derivatives of $\chi^2$ with respect to parameters $p$,

$$H_{ij} = \frac{\delta^2 \chi^2}{\delta p_i \delta p_j} \tag{3}$$

but, as is almost always done, it was calculated from

$$H_{ij} = \sum_{k=1}^{N} \left( \frac{\delta f_k^{\text{calc}}}{\delta p_i} \right) \left( \frac{\delta f_k^{\text{calc}}}{\delta p_j} \right) \tag{4}$$

The derivatives of the resonance fields, $f_k^{\text{calc}}$, with respect to the parameters $p$ had to be evaluated numerically. Errors in the best-fit parameters were finally estimated as

$$\sigma_i = \sqrt{\frac{\chi^2}{N - P} (H^{-1})_{ii}} \tag{5}$$

where $N$ is the number of experimental resonance fields and $P$ is the number of fitted parameters.

## Results

**Synthesis.** The chelating ligand Hdbm has been used in the preparation of a considerable number of high oxidation state Mn complexes with a wide range of nuclearities.[30−32] In the synthesis of such compounds, an often encountered challenge is that of preventing the formation of the very stable mononuclear tris-chelate complex $[Mn(dbm)_3]$.[3] However, it is possible to prepare in pure form the bis-chelate monomers $[MnX(dbm)_2]$ (X = Cl, Br)[31] or $[Mn(dbm)_2(py)_2](ClO_4)$ if the stoichiometry is well controlled and the appropriate terminal ligand (X or py) is present. Complex **1** was prepared in a manner very similar to that previously described.[32] The preparation consists of the generation in situ of Mn(III) in the presence of pyridine and a counterion, followed by the addition of the chelating ligand Hdbm. Given the absence of a suitable source of Mn(III) with labile ligands that is soluble in organic solvents, this ion can be formed by comproportionation of Mn(II) and Mn(VII), prior to the addition of Hdbm, according to the redox scheme

$$4\text{Mn(II)} + \text{Mn(VII)} \rightarrow 5\text{Mn(III)} \tag{6}$$

The product forms in MeCN solution and precipitates pure, with no need for recrystallization. A balanced chemical equation can be written for this transformation (eq 7). Large crystals of the compound **1** can be obtained directly from the reaction mixture if it is left unperturbed after mixing all reagents.

$$4Mn(ClO_4)_2 + Bu^n{}_4NMnO_4 + 10Hdbm + 10py \rightarrow 5[Mn(dbm)_2(py)_2](ClO_4) + Bu^n{}_4NClO_4 + 2HClO_4 + 4H_2O \tag{7}$$

**Description of the Structure.** Crystallographic data for **1** are collected in Table 1. Selected interatomic distances and angles are listed in Table 2. An ORTEP representation of the complex is shown in Figure 1.

Compound **1** is a complex of Mn(III) in an ax-$N_2$−eq-$O_4$ coordination environment. This coordination sphere is well-known for complexes formally of Mn(II), indeed with axial py and equatorial $\pi$-conjugated $O_2$ donor ligands (e.g., catecholates/quinones).[33,34] The ax-$N_2$−eq-$O_4$ coordination environment is less common for Mn(III), although there are several known examples of this donor set.[35−37] Complex **1**, however, represents the first of this coordination environment for mononuclear Mn(III) in which the axial ligands are py (or similar heterocycles) and the equatorial ligands are $\pi$-conjugated $O_2$ donors. A very similar coordination sphere has been reported for a *dinuclear* complex of Mn(III).[38]

As is often found for pseudooctahedral high-spin $d^4$ systems, complex **1** displays a static Jahn−Teller distortion in the form of a tetragonal elongation. The long axis is formed by the N−Mn vectors arising from pyridine molecules, with bond distances of 2.273(1) and 2.291(1) Å, respectively. The equatorial positions are occupied by the O-donors of two $dbm^-$ chelating ligands, featuring Mn−O bond distances in the range 1.902(1)−1.918(1) Å. The idealized planes of the pyridine groups are inclined to one another by 34.52(4)°. This is in contrast with the reported dinuclear complex $[Mn_2(L)_2(py)_4]$ ($H_3L$ = 3-(3-oxo-3phenylpropionyl)-5-methylsalicylic acid), where each Mn(III) is in the same coordination environment as in **1** but with the trans pyridine ligands almost perpendicular to each other.[38] Three of the four phenyl groups per molecule of **1** are participating in intermolecular $\pi-\pi$ stacking interactions (range of intercentroid distances 3.570−3.781 Å), thereby, each molecule being connected to two other complexes via either one or two such interactions, respectively. This supramolecular arrangement leads to infinite chains of molecules within the crystal structure, which is reminiscent of a similar organization observed in the solid state of the molecules $[MnCl(dbm)_2]$ or $[MnCl(Me_2dbm)_2]$, which are related to **1**.[31] Between the $[Mn(dbm)_2(py)_2]$ chains lie the $ClO_4^-$ counterions.

**HFEPR.** The most important aspect of HFEPR spectra of the polycrystalline complex is the complete absence of


(29) Wilkinson, J. H. *The Algebraic Eigenvalue Problem*; Clarendon Press: London, 1970.
(30) Aromí, G.; Aubin, S. M. J.; Bolcar, M. A.; Christou, G.; Eppley, H. J.; Folting, K.; Hendrickson, D. N.; Huffman, J. C.; Squire, R. C.; Tsai, H. L.; Wang, S.; Wemple, M. W. *Polyhedron* **1998**, *17*, 3005−3020.
(31) Aromí, G.; Knapp, M. J.; Claude, J. P.; Huffman, J. C.; Hendrickson, D. N.; Christou, G. *J. Am. Chem. Soc.* **1999**, *121*, 5489−5499.
(32) Wang, S.; Wemple, M. S.; Yoo, J.; Folting, K.; Huffman, J. C.; Hagen, K. S.; Hendrickson, D. N.; Christou, G. *Inorg. Chem.* **2000**, *39*, 1501−1513.
(33) Lynch, M. W.; Hendrickson, D. N.; Fitzgerald, B. J.; Pierpont, C. G. *J. Am. Chem. Soc.* **1984**, *106*, 2041−2049.
(34) Attia, A. S.; Pierpont, C. G. *Inorg. Chem.* **1995**, *34*, 1172−1179.
(35) Shongwe, M. S.; Vandayar, S. K.; Fernandes, M. A.; Marques, H. M.; Morris, M. J.; Heath, S. L. *Polyhedron* **2001**, *20*, 2195−2201.
(36) Nakamura, T.; Niwa, K.; Usugi, S.; Asada, H.; Fujiwara, M.; Matsushita, T. *Polyhedron* **2001**, *20*, 191−201.
(37) Bermejo, M. R.; Deibe, A. G.; Rey, M.; Sanmartin, J.; Sousa, A.; Aurangzeb, N.; Hulme, C. E.; McAuliffe, C. A.; Pritchard, R. G.; Watkinson, M.; Helliwell, M. *J. Chem. Soc., Dalton Trans.* **1994**, 1265−1269.
(38) Aromí, G.; Gamez, P.; Roubeau, O.; Berzal, P. C.; Kooijman, H.; Spek, A. L.; Driessen, W. L.; Reedijk, J. *Inorg. Chem.* **2002**, *41*, 3673−3683.

**Table 1.** Crystallographic Data for [Mn(dbm)$_2$(py)$_2$](ClO$_4$) (**1**)

| | |
|---|---|
| cryst shape/color | block/dark brown |
| cryst size, mm | 0.40 × 0.40 × 0.40 |
| formula | $C_{40}H_{32}ClMnN_2O_8$ |
| fw | 759.07 |
| cryst system | monoclinic |
| space group | $P2_1n$ |
| *a*, Å | 8.2851(4) |
| *b*, Å | 24.0826(9) |
| *c*, Å | 17.9576(9) |
| α, deg | 90 |
| *β*, deg | 100.144(4) |
| *γ*, deg | 90 |
| *V*, Å$^3$ | 3527.0(3) |
| *Z* | 4 |
| *T*, K | 153.2 |
| $\rho_{calc}$, g/cm$^3$ | 1.429 |
| wavelength (Mo Kα), Å | 0.710 73 |
| $\mu$, mm$^{-1}$ | 0.508 |
| unique data | 9792 |
| R,[a] wR2[b] ($I > 2\sigma(I)$) | 0.0367, 0.0935 (8317 reflns) |

[a] $R = \Sigma||F_o| - |F_c||/\Sigma|F_o|$. [b] $wR2 = [\Sigma[w(F_o^2 - F_c^2)^2]/\Sigma[w(F_o^2)^2]]^{1/2}$.

**Table 2.** Selected Bond Distances (Å) and Angles (deg) for [Mn(dbm)$_2$(py)$_2$](ClO$_4$) (**1**)

| | | | |
|---|---|---|---|
| Mn(1)−O(4) | 1.902(1) | Mn(1)−O(2) | 1.918(1) |
| Mn(1)−O(3) | 1.910(1) | Mn(1)−N(2) | 2.273(1) |
| Mn(1)−O(1) | 1.910(1) | Mn(1)−N(1) | 2.291(1) |
| O(4)−Mn(1)−O(3) | 92.67(4) | O(1)−Mn(1)−N(2) | 94.17(4) |
| O(4)−Mn(1)−O(1) | 87.04(4) | O(2)−Mn(1)−N(2) | 87.36(5) |
| O(3)−Mn(1)−O(1) | 174.98(5) | O(4)−Mn(1)−N(1) | 90.73(4) |
| O(4)−Mn(1)−O(2) | 174.87(5) | O(3)−Mn(1)−N(1) | 88.96(4) |
| O(3)−Mn(1)−O(2) | 89.13(4) | O(1)−Mn(1)−N(1) | 86.03(4) |
| O(1)−Mn(1)−O(2) | 91.58(4) | O(2)−Mn(1)−N(1) | 94.10(4) |
| O(4)−Mn(1)−N(2) | 87.82(5) | N(2)−Mn(1)−N(1) | 178.53(5) |
| O(3)−Mn(1)−N(2) | 90.83(4) | | |

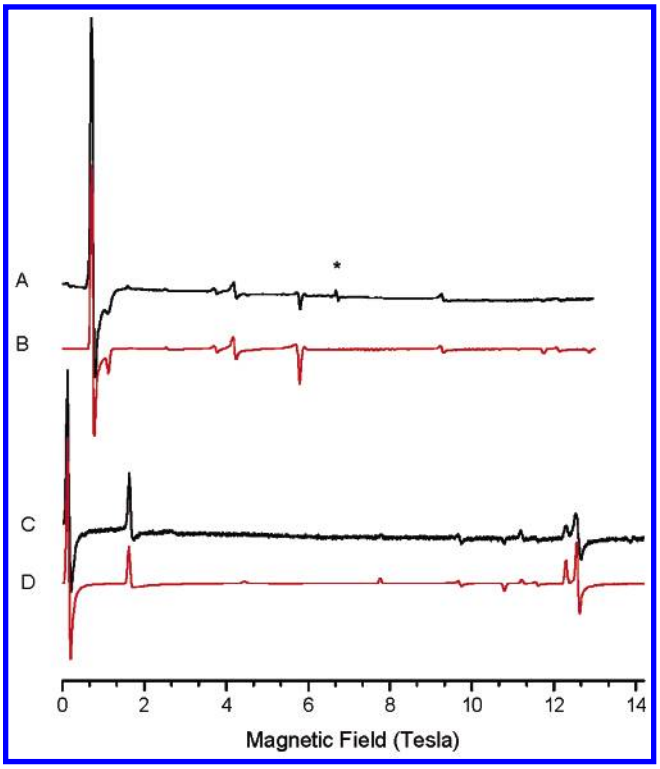


**Figure 3.** HFEPR spectra of solid polycrystalline **1** at two selected frequencies and their simulations: (A) experiment at 187.51 GHz and 40 K; (B) simulation at the same conditions as A; (C) experiment at 438.15 GHz and 40 K; (D) simulation at the same conditions as C. Spectra B and D were simulated using spin Hamiltonian parameters as given in Table 3. The line marked with an asterisk originates from a Mn(II) impurity and is not reproduced in the simulations.

any field-induced torquing phenomena, which occur very frequently in other solid Mn(III) complexes.[10] This results in perfect powder spectra, free of artifacts, and allows the experimentalist to work with the solid "as is" without a need to implement crystallite-constraining methods. Spectra could be recorded in the 4.2−77 K temperature range, with signal-to-noise ratio very good at low temperatures, but becoming progressively worse at the upper limit of that range. No temperature-dependent changes in the spectra other than intensity were observed. Figure 3 shows HFEPR spectra at 40 K of polycrystalline complex **1** recorded at two selected frequencies accompanied by simulations assuming a perfectly random orientation of the crystallites with regard to the magnetic field. (The simulation parameters were obtained from a multifrequency dataset in a method described before and not from individual spectra.) A striking feature of Figure 3 is the nearly prefect agreement between the simulations and the experiments not only in terms of the position of the resonances but also their shape and intensity, which confirms the absence of field-induced artifacts. This agreement persists to the highest frequencies and fields used in this work (440 GHz, and 15 T, respectively). Indeed, the best spectra were obtained at the highest limit of the available frequency range.

As some of us argued elsewhere,[6] the magnetic properties of a given complex in a solid not only depend on its intrinsic characteristics but are often influenced by the properties of the crystal lattice. It is therefore desirable to carry out an experiment on a complex isolated in an "inert" (noncoordinating) solvent, necessarily here as a frozen solution, to eliminate the unwanted crystal effects. We have thus performed HFEPR measurements on **1** dissolved in $CH_2Cl_2$ in a concentration of about 100 mM. The resulting spectra are shown in Figure 4, at two selected frequencies, accompanied again by simulations assuming a perfectly random orientation of the molecules with regard to the field. The very good agreement between the simulations and the experiment indicates a high quality of the frozen solution; however, the spectra also show a line-broadening effect compared to the solid state. Most importantly, there is very little difference in spin Hamiltonian parameters between the solid and the frozen solution, which proves that $CH_2Cl_2$ is an "innocent" solvent for **1** and also that the properties of the complex in its solid form are not determined by the crystal packing constraints or similar factors.[39]

Rather than extracting spin Hamiltonian parameters by fitting them to individual single-frequency spectra, as is usually done in EPR, we collected all the observed resonances at multiple frequencies in a single 2-D array (resonance fields as function of sub-THz quantum energy), which is indicated by squares in Figure 5 for the case of polycrystalline **1**. We have previously used this procedure for triplet ($S = 1$) spin systems, such as molecular oxygen,[23]

(39) HFEPR spectra for **1**, either as a solid or diluted in frozen solution, do not exhibit resolved hyperfine splitting from $^{55}$Mn, in concurrence with all other HFEPR studies of Mn(III) molecular complexes known to us.

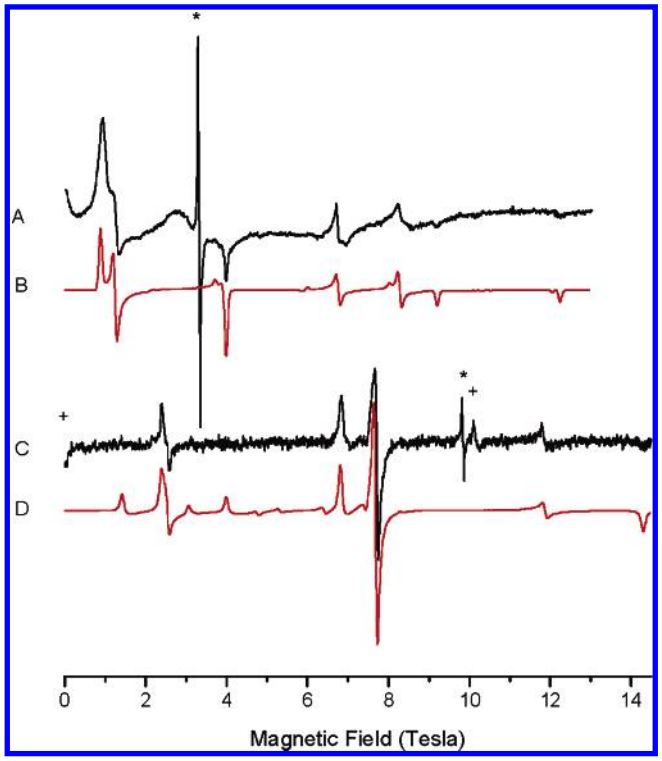


**Figure 4.** HFEPR spectra of a solution of **1** in methylene chloride at two selected frequencies and their simulations: (A) experiment at 92.818 GHz and 30 K; (B) simulation at the same conditions as A; (C) experiment at 273.45 GHz; (D) simulation at the same conditions as C. Spectra B and D were simulated using spin Hamiltonian parameters as given in Table 3. The line marked with an asterisk originates from a Mn(II) impurity while the lines marked with crosses are generated by the fourth harmonic of the fundamental frequency. Neither of these lines are reproduced in the simulations.

high-spin Ni(II),[40] and V(III),[41] as well as for a quartet ($S = {}^3/_2$), Co(II).[42] A quintet spin state ($S = 2$), particularly with rhombic symmetry, as studied here, however, displays many more possible transitions than does a spin triplet or quartet. Consequently, we employed the software as described in the Experimental Section to extract spin Hamiltonian parameters from the complete 2-D dataset. This approach ensures that an equally optimal fit is achieved at any frequency and allows one to rigorously calculate the experimental error from the statistical analysis.[43]

For the polycrystalline sample of **1**, a very satisfactory agreement was found between the experimental and simulation resonant fields using the set of spin Hamiltonian parameters including only the Zeeman term and second-order zero-field splitting terms $D$ and $E$ (rms = 48 mT). However, if fourth-order terms of the Hamiltonian (eq 1) are included, then the agreement becomes significantly better (rms = 16 mT). In particular, both the parameters $B_4^2$ and $B_4^4$ are nonnegligible. Parameter $B_4^2$ of 0.0007(3) cm$^{-1}$ is relatively

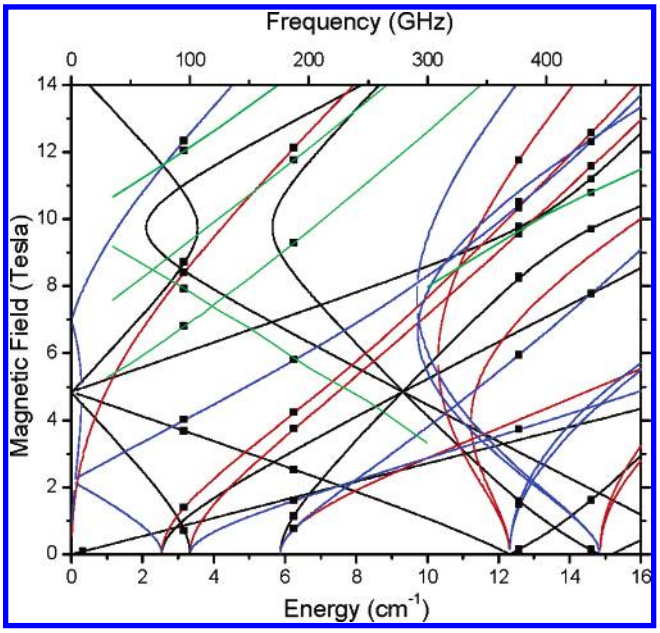


**Figure 5.** Dependence of the resonance fields on sub-THz quantum energy in polycrystalline **1**. The squares represent the experimental resonances including the single "non-Kramers" line observed at X-band, while the lines were drawn using the spin Hamiltonian parameters as in Table 3, including the fourth-order terms. The red lines are the *x* canonical turning points in the powder pattern, the blue lines are the *y* turning points, and the black lines are the *z* turning points, while the green lines represent the off-axis turning points.

strongly correlated with $E$ (correlation coefficient 0.604; see Supporting Material), which is not surprising as their respective operators, $O_2^2$ and $O_4^2$, both contain terms in [$\mathbf{S}_+^2 + \mathbf{S}_-^2$], and is probably the reason $B_4^2$ is rarely reported. Parameter $B_4^4$, on the other hand, is only weakly correlated with the other Hamiltonian terms and is significantly different from zero, taking a value 0.0048(4) cm$^{-1}$. The actual correlation matrix (see Supporting Material) indicates no excessive dependencies among other parameters in the solid sample.

The final fit quality can be judged visually by comparing the experimental resonances (squares in Figure 5) with the simulated curves (lines in Figure 5). The effect of fourth-order parameters on improving the fits was also observable in single-frequency spectra. Particular transitions are sensitive to fourth-order zfs parameters to a varying degree. We found the strongest dependence in spectra obtained at 377 GHz, as shown in Figure 6, which presents the high-field part of an EPR spectrum of polycrystalline **1** and compares it to spectra simulated by using the best-fit parameters with fourth-order zfs terms either present or absent. Clearly, a better agreement is achieved when the fourth-order zfs terms are included in the simulations. The final set of spin Hamiltonian parameters for solid **1** is shown in Table 3. For the frozen-solution spectra, an analogous analysis of a 2-D dataset was performed, and the spin Hamiltonian parameters obtained from it are also given in Table 3. Extraction of fourth-order zfs parameters, however, was not successful in the frozen solution, since the statistical error was on the order of, or even larger than, the parameters themselves (Table 3). This was primarily caused by the increased line width of the solution resonances compared to the solid-state spectra,

(40) Krzystek, J.; Park, J.-H.; Meisel, M. W.; Hitchman, M. A.; Stratemeier, H.; Brunel, L.-C.; Telser, J. *Inorg. Chem.* **2002**, *41*, 4478−4487.
(41) Krzystek, J.; Fiedler, A. T.; Sokol, J. J.; Ozarowski, A.; Zvyagin, S. A.; Brunold, T. C.; Long, J. R.; Brunel, L.-C.; Telser, J. *Inorg. Chem.* **2004**, *43*, 5645−5658.
(42) Krzystek, J.; Zvyagin, S. A.; Ozarowski, A.; Fiedler, A. T.; Brunold, T. C.; Telser, J. *J. Am. Chem. Soc.* **2004**, *126*, 2148−2155.
(43) Tregenna-Piggott, P. L. W.; Weihe, H.; Barra, A.-L. *Inorg. Chem.* **2003**, *42*, 8504−8508.

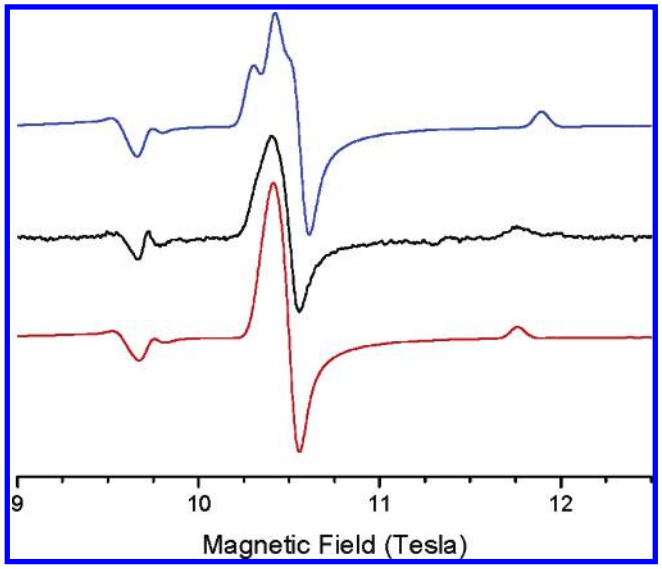


**Figure 6.** High-field part of a HFEPR spectrum of polycrystalline **1** at 377.3 GHz. For transition identification, one should draw a vertical line in Figure 5 corresponding to the experimental frequency. The middle (black) trace is the experiment. The uppermost (blue) trace was simulated with the following best-fit spin Hamiltonian parameters without fourth-order terms: $D = -4.509$ cm$^{-1}$; $E = -0.422$ cm$^{-1}$; $g_x = 1.989$; $g_y = 1.994$; $g_z = 1.983$. The lowest (red) trace was simulated with the best-fit parameters that did include fourth-order terms as given in Table 3.

which made the accurate determination of particular turning points more difficult than in the solid sample. Also, fewer data points were collected in the case of the frozen solution than for the solid sample.

## Discussion

The HFEPR spectra of the solid polycrystalline **1** are remarkable for their high quality, which is at least partly due to the absence of any field-induced torquing effects. This results in a system that can be considered as a model rhombic $S = 2$ spin complex and can be measured as a solid without any preparation of the sample to yield repeatable and highly accurate results.

The high quality of the HFEPR data allowed us for the first time—to our best knowledge—to determine the fourth-order zfs parameters of an $S = 2$ spin system from powder spectra. In particular, both parameters $B_4^2$ and $B_4^4$ were found to be significantly different from zero, $7(3) \times 10^{-4}$ and $48(4) \times 10^{-4}$ cm$^{-1}$, respectively (the other fourth-order parameter, $B_4^0$, is zero within statistical error). $B_4^2$ appears to be correlated with $E$, however, which is probably the reason it is rarely considered. Previously, fourth-order zfs parameters in a $S = 2$ system could be extracted exclusively from single-crystal spectra.[4,14] Although the determination of the fourth-order zfs parameters could be considered an academic enterprise, these terms of the spin Hamiltonian may be significant in specific cases, as in high-spin molecular clusters such as $Mn_{12}$, where they were proposed to influence quantum tunneling probability between the particular $\pm M_S$ states through breaking the symmetry of the zfs tensor.[44] It is thus reassuring that the fourth-order parameters extracted by us for the mononuclear Mn(III) complex, **1**, from its powder HFEPR spectra fall within the same range as determined in the two cases for Mn(III) studied by single-crystal EPR. In the case of the [Mn(cyclam)Br$_2$]Br complex, $B_4^4$ was also established as the largest of the three fourth-order parameters and found positive[14] as in the case of **1** ($17 \times 10^{-4}$ vs $48 \times 10^{-4}$ cm$^{-1}$). In the case of Mn(III) in rutile, only the cubic parameter $a$ was reported and was equal to 0.13 cm$^{-1}$,[4] which when recalculated into the $B_4^m$ parameters, assuming cubic symmetry, yields $B_4^0 = 11 \times 10^{-4}$, equivalent to $B_4^4 = 55 \times 10^{-4}$ cm$^{-1}$, which is in good agreement with $B_4^4 = 48 \times 10^{-4}$ cm$^{-1}$ determined for complex **1**. Also, although we were unable to accurately determine fourth-order zfs parameters in the complex Mn(acac)$_3$, whose second-order zfs values are very close to those of complex **1**,[6] the estimate of the cubic parameter $a \approx 0.15$ cm$^{-1}$ yields $B_4^4 \approx 63 \times 10^{-4}$ cm$^{-1}$, again in reasonable agreement with the value of $48 \times 10^{-4}$ cm$^{-1}$ found in complex **1**.

The accurate determination by HFEPR of not only second-order but also fourth-order zfs parameters of the spin Hamiltonian for a quintet ($S = 2$) state is quite instructive as to the perils of determining these parameters from single-frequency spectra, particularly those obtained at low frequencies, such as 9.5 GHz typical for X-band EPR. We have shown previously that such a procedure when applied to a Mn(III) complex leads to underdetermination;[6] that is, different sets of parameters may equally well simulate a given "non-Kramers" X-band signal. In the case of complex **1**, the non-Kramers signal at X-band is only weakly dependent on the fourth-order zfs parameters, so that their inclusion in the simulation leads to a shift of the resonance amounting to ca. 4 mT (from 87 to 83 mT at 9.45 GHz) compared to the line width of ca. 25 mT. As shown in Figure 6, certain resonances appearing at much higher frequencies are more sensitive to fourth-order zfs parameters, as their inclusion in the simulations leads to spectral shifts as large as 150 mT compared to experimental line widths on the order of 50 mT. HFEPR is thus inherently more accurate in determining spin Hamiltonian parameters in high-spin rhombic Mn(III) complexes (and other high-spin systems characterized by large zfs anisotropy) than conventional EPR spectroscopy, provided the line widths and line shapes are sufficiently narrow and well-defined to allow a precise reading of the resonance field position.

**Table 3.** Spin Hamiltonian Parameters for **1** Obtained from a Simultaneous Least-Squares Fit to the Complete Dataset for the Polycrystalline Solid (Represented by Squares in Figure 5) and an Analogous Dataset Collected for the Solution (Not Shown)

| | $D$ (cm$^{-1}$) | $E$ (cm$^{-1}$) | $B_4^0$ ($10^{-4}$ cm$^{-1}$) | $B_4^2$ ($10^{-4}$ cm$^{-1}$) | $B_4^4$ ($10^{-4}$ cm$^{-1}$) | $g_x$ | $g_y$ | $g_z$ |
|---|---|---|---|---|---|---|---|---|
| polycryst | −4.504(2) | −0.425(1)[a] | −1.8(4) | 7(3) | 48(4) | 1.993(1) | 1.994(1) | 1.983(1) |
| soln | −4.500(8) | −0.430(5) | 0(1) | −3(12) | 18(17) | 1.990(4) | 1.978(5) | 1.972(5) |

[a] Because the choice of the sign of $E$ is arbitrary, we followed a convention that attributes to $E$ the same sign as of the parameter $D$, i.e., in our case negative. Changing the sign of $E$ would require a corresponding permutation of the $g_x$ and $g_y$ values.

**Table 4.** Summary of Spin Hamiltonian Parameters for Mn(III) Complexes

| coord sphere | complex | $D$ ($cm^{-1}$) | $E$ ($cm^{-1}$) | $B_4^0$ ($10^{-4}$ $cm^{-1}$) | $B_4^2$ ($10^{-4}$ $cm^{-1}$) | $B_4^4$ ($10^{-4}$ $cm^{-1}$) | $g_x$ | $g_y$ | $g_z$ |
|---|---|---|---|---|---|---|---|---|---|
| $N_6$ | $Mn(terpy)(N_3)_3$[a] | −3.29(1) | 0.51(1) | | | | 2.000(5) | 1.980(5) | 2.010(5) |
| | $Mn(bpea)(N_3)_3$[b] | +3.50(1) | 0.82(1) | | | | 2.02(1) | 1.98(1) | 1.95(1) |
| $N_4Br_2$ | $[Mn(cyclam)Br_2]Br$[c] | −1.1677(7) | −0.0135(6) | 9(3) | 6(2) | 17(3) | 2.005(4 ) | 2.036(2 ) | 2.015(2) |
| $N_4I_2$ | $Mn(cyclam)I_2$[d] | +0.604 | 0.034 | | | | 2.00 | 2.00 | 1.99 |
| $N_4Cl$ | Mn(TPP)Cl[e] | −2.290(5) | 0.00(1) | | | | 2.005(3 ) | 2.005(3 ) | 1.98(2) |
| | Mn(Pc)Cl[e] | −2.31(1) | 0.00(1) | | | | 2.005(5 ) | 2.005(5 ) | 2.00(2) |
| | Mn(ODMAPz)Cl[f] | −2.33(1) | 0.00(1) | | | | | | 1.984 |
| | Mn(OEP)Cl[g] | −2.40(1) | ≤0.02(1) | | | | 2.00(1) | 2.00(1) | 2.00(1) |
| | Mn(TSP)[h] | −3.12(2) | 0.00(1) | | | | 2.00(2) | 2.00(2) | 2.00(2) |
| $N_4Br$ | Mn(OEP)Br[g] | −1.07(1) | 0.00(1) | | | | 2.01(1) | 2.01(1) | 1.98(1) |
| $N_4O$ | $Mn(tpfc)(OPPh_3)$[i] | −2.69(2) | 0.030(3) | | | | 1.994(4 ) | 1.994(4) | 1.980(4) |
| $N_4$ | Mn(cor)[j] | −2.64(1) | 0.015(5) | | | | 2.02(1) | 2.02(1) | 2.00(1) |
| $N_3F_3$ | $Mn(terpy)F_3$[b] | −3.82(2) | 0.75(2) | | | | 1.97(2) | 2.04(1) | 1.96(1) |
| | $Mn(bpea)F_3$[b] | −3.67(2) | 0.70(2) | | | | 1.96(1) | 1.98(1) | 1.98(1) |
| $N_2O_2C$ l | Mn(salen)[h] | −2.47(2) | 0.17(1) | | | | 2.00(2) | 2.00(2) | 2.00(2) |
| $N_2O_4$ | $[Mn(dbm)_2(py)_2](ClO)_4$[k] | −4.504(2) | −0.425(1) | −1.8(4) | 7(3) | 48(4) | 1.993(1 ) | 1.994(1) | 1.983(1) |
| $O_6$ | $Mn(dbm)_3$[l] | −4.35 | 0.26 | | | | 1.99 | 1.99 | 1.97 |
| | $Mn(acac)_3$[m] | −4.52(2) | 0.25(2) | | | | 1.99(1) | 1.99(1) | 1.99(1) |
| | $CsMn(SO_4)_2 \cdot 12D_2O$[n] | −4.524(1) | 0.276(1) | | | | | | |
| | $CsMn(SO_4)_2 \cdot 12D_2O$[o] | −4.491(7) | 0.248(5) | | | | 1.981(5 ) | 1.993(5) | 1.988(5) |
| | $CsMn(SO_4)_2 \cdot 12H_2O$[o] | −4.431(9) | 0.258(8) | | | | 2.001(5) | 1.997(7) | 1.966(12) |
| | $Mn^{3+}$ in $TiO_2$[p] | −3.4(1) | 0.116(1) | 11 | | 55 | 2.00(2) | 2.00(2) | 1.99(1) |
| $O_4Cl$ | $Mn(Me_2dbm)Cl$[g] | −2.45(3) | 0.00(1) | | | | 2.03(2) | 2.03(2) | 2.02(2) |
| $O_4Br$ | $Mn(Me_2dbm)Br$[g] | −1.40(2) | 0.00(1) | | | | 1.98(2) | 1.98(2) | 1.98(2) |

[a] Reference 11. [b] Reference 12. [c] Reference 14. [d] Reference 13. [e] Reference 10. [f] Reference 2. A complex with another axial ligand, DTC, is also reported. [g] Reference 7. An analogous complex with iodine is also described. [h] Reference 16. [i] Reference 9. [j] Reference 8. [k] This work. [l] Reference 3. [m] Reference 6. [n] Reference 5. These workers employed zero-field inelastic neutron scattering (INS), which directly provides the zfs parameters but gives no information on $g$ values. [o] Reference 43. [p] Reference 4. These authors reported the cubic fourth-order zfs parameter $a$ equal to 0.13 $cm^{-1}$, which we recalculated along the convention we use with an assumption of a cubic symmetry. See note 25.

The successful determination of the fourth-order zfs terms and the high precision obtained for the other spin Hamiltonian parameters ($2 \times 10^{-3}$ $cm^{-1}$ for $D$, $1 \times 10^{-3}$ $cm^{-1}$ for $E$, and $1 \times 10^{-3}$ for the **g** matrix values) was possible not only because of the high spectral quality but also through the use of a novel software. Traditionally, spin Hamiltonian parameters were fitted to single-frequency spectra in EPR because most spectrometers operated at a single (low) frequency. With the advent of HFEPR it was realized that truly optimal parameters were those that fit several frequencies, particularly for high-spin systems. A multifrequency approach was thus adopted,[44] with the spectra recorded at several frequencies and the Hamiltonian parameters fitted to them for the most part using human judgment. Since human judgment has its limitations, it was not unusual to report parameters that were not entirely frequency-independent but allowed for some variation depending on the frequency. The methodology that we report here was previously used by some of us in determining Hamiltonian parameters in $S = 1$ systems such as Ni(II), V(III), and molecular oxygen[23,40,41]and subsequently also in a $S = {}^3/_2$ system, Co(II).[42] Very recently it was employed in a $S = 2$ system (high-spin Fe(II)).[45] A similar approach has been used by Tregenna-Piggott et al.[43,46] and by Mossin et al.[14] The method depends on collecting all the observed resonances in a 2-D array (resonant field vs transition energy) and fitting the Hamiltonian parameters simultaneously to the complete dataset, as opposed to individual spectra. This approach ascertains that the equally optimal fit is achieved at any frequency and allows one to rigorously calculate the experimental error from the statistical analysis. This is particularly important in the quintet spin state ($S = 2$) as studied here, since many more possible transitions between the spin sublevels are observed than in a triplet or a quartet, making the field vs energy diagrams such as the one shown in Figure 5 much more complicated than for $S = 1$ or $S = {}^3/_2$. In addition to a vastly increased number of canonical resonances, the quintet state powder pattern contains multiple off-axis turning points (green lines in Figure 5), which were used in the fits along with the canonical orientations. The resulting agreement between the experiment and simulation can be judged from both single-frequency spectra (Figures 3 and 6 for the solid, Figure 4 for the frozen solution) and the multifrequency dataset (Figure 5, solid only; the frozen solution produced an analogous dataset, and the agreement was almost as good).

The large amount of data obtained by HFEPR and other techniques, such as INS,[5] allows us to survey qualitatively the relation between structure and spin Hamiltonian parameters for a variety of Mn(III) complexes, which are summarized in Table 4. The zfs parameters are most informative in this regard, as described below. In principle, the $g$ values could also be correlated with molecular and electronic structure; however, this is not apparent. In all of these complexes of Mn(III), both the isotropic deviation from $g_e$ (2.00) and anisotropy in $g$ are minimal: the $g$ values range overall between 1.95 and 2.03 but are normally $1.99 \pm 0.02$.

One major structural type of Mn(III) complexes is square-pyramidal, with either bidentate or macrocyclic equatorial

(44) Barra, A.-L.; Brunel, L.-C.; Gatteschi, D.; Pardi, L.; Sessoli, R. *Acc. Chem. Res.* **1998**, *31*, 460−466.
(45) Ozarowski, A.; Zvyagin, S. A.; Reiff, W. M.; Telser, J.; Brunel, L. C.; Krzystek, J. *J. Am. Chem. Soc.* **2004**, *126*, 6574−6575.
(46) Tregenna-Piggott, P. L. W.; Weihe, H.; Bendix, J.; Barra, A.-L.; Güdel, H.-U. *Inorg. Chem.* **1999**, *38*, 5928−5929.

ligands and a variety of axial ligation. Complexes with axial chloride are all characterized by strictly axial zfs tensors ($E = 0$ within experimental error) with the zfs parameter $D$ ranging from $-2.30$ to $-2.50$ cm$^{-1}$, regardless of whether the equatorial coordination is $N_4$ (porphyrinic) or $O_4$ (bis(diketonate)).[47] Replacing the porphyrinic ligands with corroles increases the magnitude of $D$ to $-2.60$ to $-2.70$ cm$^{-1}$ [8,9] and introduces a small nonzero $|E|$ of 0.015−0.030 cm$^{-1}$ due to reduced symmetry of the corrole macrocycle. A combination of N and O donors in the equatorial coordination sphere, as in Mn(salen) ($N_2O_2Cl$),[16] preserves the $D$ value of about $-2.50$ cm$^{-1}$ but introduces a moderate rhombicity of $E = -0.17$ cm$^{-1}$.

The other major structural type of Mn(III) complexes is distorted octahedral. The most common among these is the $O_6$ coordination sphere, corresponding to a tetragonally elongated octahedron. Regardless of whether the coordination is by tris(diketonates) or hexaaqua ligands, these complexes are characterized by a $D$ between $-4.35$ and $-4.52$ cm$^{-1}$ and a moderate $E$ very close to $-0.25$ cm$^{-1}$.[48] The complex of interest here, **1**, despite having a mixed donor set (axial $N_2$, equatorial $O_4$) fits within this range of $D$ as well. The class of complexes characterized by the coordination sphere of $N_6$ and $N_3F_3$[11,12] displays $D$ on the order of $-3.30$ to $-3.80$ cm$^{-1}$. The very low symmetry of these complexes causes a strong rhombicity of the zfs tensor, with $|E|$ varying from ca. 0.50 to 0.80 cm$^{-1}$. In one particular case, this results in the change of sign of $D$, which for Mn(bpea)($N_3$)$_3$ becomes $+3.50$ cm$^{-1}$.[12] Finally, introducing a heavy atom into the coordination sphere of Mn(III) results in pronounced changes of $D$, due to the significant spin−orbit coupling attendant with heavy atoms, even when they are present only as ligands.[13] Thus, in the three known instances where Br was coordinated to Mn(III), $N_4Br$ and $O_4Br$[7] and $N_4Br_2$,[14] the magnitude of $D$ is significantly reduced to between $-1.07$ and $-1.40$ cm$^{-1}$. The presence of iodine in the coordination sphere influences the zfs parameters even further, with $D$ close to zero in Mn(OEP)I[7] and achieving a positive value ($+0.604$ cm$^{-1}$) in Mn(cyclam)$I_2$.[13]

Ideally, the spin Hamiltonian parameters derived from analysis of the HFEPR data should also be correlated with electronic energy levels obtained from optical spectroscopy. For example, in their study of the cesium manganese alum ($CsMn(SO_4)_2\cdot 12[H,D]_2O$), Tregenna-Piggott et al. also recorded variable-temperature, single-crystal electronic absorption spectra that clearly showed two ligand-field bands, one in the NIR at 10 400 cm$^{-1}$ (960 nm) and one in the visible region at 21 140 cm$^{-1}$ (470 nm).[43] The hexaaqua Mn(III) cation has octahedral symmetry that is reduced to $S_6$ due to the aqua ligands, and Jahn−Teller distortion further lowers the symmetry to $C_i$.[49] The NIR band was thus assigned to $^5A_g \rightarrow {}^5A_g$ ($C_i$), which corresponds to the tetragonal splitting within the $^5E_g$ (in $O_h$ or $S_6$ symmetry) undistorted ground state, and the visible band was assigned to $^5A_g \rightarrow {}^5T_{2g}$ ($O_h$), which corresponds to the octahedral splitting (in strong-field notation: $t_2^3e^1 \rightarrow t_2^2e^2$), wherein the deviations from octahedral symmetry were not resolved.[43] These assignments, combined with the extensive data available for aqua ligands, allowed these workers to estimate the bonding parameters (using the AOM apparatus[50]) of the axial and equatorial aqua ligands in $[Mn([H,D]_2O)_6]^{3+}$, which could then be used in combination with estimates for the Racah and spin−orbit coupling parameters to calculate values for spin Hamiltonian parameters in excellent agreement with experiment.[43]

An analogous analysis is exceedingly difficult here. Unlike aqua complexes, the electronic absorption spectrum of metal diketonates is dominated by charge-transfer and/or $\pi-\pi^*$ transitions involving the $\pi$-conjugated ligands. Nevertheless, for Mn(acac)$_3$ and various other tris($\beta$-diketonates) and related complexes (e.g., $K_3Mn(ox)_3$, ox = $C_2O_4^{2-}$), it is possible to observe a ligand-field (d−d) transition in the NIR region, which is assigned in $D_{4h}$ symmetry to $^5B_{1g} \rightarrow {}^5A_{1g}$ (i.e., the tetragonal splitting of $^5E_g$).[51] Two features in the visible region are also observed that can be assigned to ligand-field transitions: $^5B_{1g} \rightarrow {}^5B_{2g}$; $^5B_{1g} \rightarrow {}^5E_g$. These three bands allow a unique determination of the three Ballhausen[52] tetragonal crystal-field parameters, *Dq*, *Ds*, and *Dt*.[51] Use of these parameters for Mn(acac)$_3$ in combination with the Racah and spin−orbit parameters employed for $[Mn(H_2O)_6]^{3+}$ (∼80% of the free-ion values), yields an axial zfs parameter, $D \approx -3.7$ cm$^{-1}$, with a small cubic component ($a \approx 0.06$ cm$^{-1}$), reasonably close to that determined here for **1**.

Thus, the electronic absorption features observed for **1** in the range 480−520 nm (∼20 000 cm$^{-1}$) could likewise be assigned to $^5E_g \rightarrow {}^5T_{2g}$ transitions in $O_h$ symmetry so that the octahedral splitting in $[Mn(dbm)_2(py)_2]^+$ is indeed similar to that in $[Mn(H_2O)_6]^{3+}$ and Mn(III) tris($\beta$-ketonate) complexes. However, in contrast to these complexes, no bands are visible in the NIR region that would shed light onto the magnitude of tetragonal splitting in $[Mn(dbm)_2(py)_2]^+$ to enable a calculation using a crystal-field model, which could refine the calculation described above.

A better method, in any case, is to use the AOM, as was done for the aqua complexes.[43] Unfortunately, complex **1** is heteroleptic, which increases the number of AOM bonding parameters; moreover, the pyridine and dbm ligands are inherently much more complex than the aqua ligand, due to their $\pi$-conjugation (the Orgel effect).[53] Therefore, we can only note the remarkable similarity in $D$ values between $[Mn(dbm)_2(py)_2]^+$ and $[Mn([H,D]_2O)_6]^{3+}$,[5,43] as well as the $\beta$-diketonate complexes with $O_6$ coordination: Mn(acac)$_3$,[6] and Mn(dbm)$_3$.[3] Indeed, as seen from Table 3, the difference in $D$ values between $[Mn(dbm)_2(py)_2]^+$ and $[Mn(D_2O)_6]^{3+}$, both as determined by HFEPR, is less than the difference in

(47) There is a sole exception to this rule: the complex tetraphenylsulfonateporphyrinatoMn(III) has a much larger magnitude of $D$ equal to $-3.12$ cm$^{-1}$ [16] but still a rigorously axial zfs tensor.
(48) An exception is found for Mn(III) as a dopant in rutile, but this is not a molecular complex.
(49) Tregenna-Piggott, P. L. W.; Andres, H.-P.; McIntyre, G. J.; Best, S. P.; Wilson, C. C.; Cowan, J. A. *Inorg. Chem.* **2003**, *42*, 1350−1365.
(50) Schäffer, C. E. *Struct. Bonding* **1968**, *5*, 68−95.
(51) Davis, T. S.; Fackler, J. P., Jr.; Weeks, M. J. *Inorg. Chem.* **1968**, *7*, 1994−2002.
(52) Ballhausen, C. J. In *Introduction to Ligand Field Theory*; McGraw-Hill: New York, 1962; pp 99−103.
(53) Schäffer, C. E.; Yamatera, H. *Inorg. Chem.* **1991**, *30*, 2840−2853.

*D* values for $[Mn(D_2O)_6]^{3+}$, as determined by HFEPR[43] versus INS.[5] Likewise, the difference in *D* values between the protio and deuterio hexaaqua Mn(III) cations is greater than the difference in *D* values between $[Mn(dbm)_2(py)_2]^+$ and $[Mn(D_2O)_6]^{3+}$. Thus the AOM parameters determined for $[Mn(H_2O)_6]^{3+}$, $e_{(\sigma,\pi)}^{ax,\ eq}$,[43] would produce the *D* value for $[Mn(dbm)_2(py)_2]^+$, simply by relabeling the parameters as $e_{(\sigma,\pi)}^{py}$ and $e_{(\sigma,\pi)}^{dbm}$, respectively.

The sole difference between $[Mn(dbm)_2(py)_2]^+$ and the homoleptic diketonate or aqua complexes is the larger value for the rhombic zfs, *E*, in **1**. The origin of *E* was discussed by Tregenna-Piggott and co-workers in their study of $[Mn([H,D]_2O)_6]^{3+}$, who quantitatively related its magnitude to the aqua ligand twist angle, $\varphi$.[43] Given that we have no independent basis for estimation of the AOM parameters in $[Mn(dbm)_2(py)_2]^+$, we simply note that the axial pyridine ligands exhibit a significant twist with respect to the equatorial plane, as described above in the description of the molecular structure, and this effect could be responsible for the marked rhombicity of the zfs tensor. The phase-coupling of the equatorial dbm ligands[54] could also play a role in enhancing the rhombic splitting.

## Conclusions

A mononuclear complex of Mn(III), $[Mn(dbm)_2(py)_2](ClO_4)$, **1**, was prepared and structurally characterized. The complex has axial pyridine ligands and equatorial O-donor ligands within a $\pi$ conjugated system, which represents a structural type that has been reported in many instances for Mn(II) but not for mononuclear Mn(III). Very high quality HFEPR spectra were recorded for **1** as both a polycrystalline solid and in $CH_2Cl_2$ frozen solution over a wide range of frequencies in the sub-THz regime. The complete dataset of resonant magnetic fields versus sub-THz quantum energy was analyzed using an automated fitting software. This analysis yielded the following spin Hamiltonian parameters (energies in $cm^{-1}$): $D = -4.504(2)$, $E = -0.425(1)$, $B_4^0 = -1.8(4) \times 10^{-4}$, $B_4^2 = 7(3) \times 10^{-4}$, $B_4^4 = 48(4) \times 10^{-4}$, $g_x = 1.993(1)$, $g_y = 1.994(1)$, and $g_z = 1.983(1)$, where the $B_4^n$ values represent fourth-order zero-field splitting terms that are generally difficult to extract from experiment and usually available only from sophisticated single-crystal measurements. The present results demonstrate the applicability of HFEPR to high-precision measurements, even for polycrystalline samples in propitious cases such as complex **1**.

Comparison with other six-coordinate complexes of Mn(III), in particular hexaaqua and tris($\beta$-diketonate) complexes suggests that the electronic structure of all of these shows a truly remarkable commonality, despite distinct variation in ligation.

**Acknowledgment.** We acknowledge the Spanish Ministry of Science and Technology for the contract "Ramón y Cajal" (G.A.) and the Swiss National Science Foundation (H.-M.S.-E.). The NHMFL is funded by the NSF through the Cooperative Agreement No. DMR-0084173 and the State of Florida.

**Supporting Information Available:** An X-ray CIF file, the details of powder spectra simulations, and the Hessian and correlation matrices resulting from the statistical analysis of HFEPR dataset. This material is available free of charge via the Internet at http://pubs.acs.org.

IC049180U

(54) Ceulemans, A.; Dendooven, M.; Vanquickenborne, L. G. *Inorg. Chem.* **1985**, *24*, 1153−1158.